J|A|C|S COMMUNICATIONS

Published on Web 06/10/2010

Ultrafast Photodriven Intramolecular Electron Transfer from a Zinc Porphyrin to a Readily Reduced Diiron Hydrogenase Model Complex

Amanda P. S. Samuel, Dick T. Co, Charlotte L. Stern, and Michael R. Wasielewski*

Department of Chemistry and Argonne−Northwestern Solar Energy Research (ANSER) Center, Northwestern University, Evanston, Illinois 60208-3113

Received January 1, 2010; E-mail: m-wasielewski@northwestern.edu

The development of molecular systems that utilize earth-abundant first-row transition metals for the photogeneration of H_2 has received increased attention in recent years.[1−8] In general, such systems are composed of a proton reduction catalyst, a chromophore that serves to harvest light and transfer reducing equivalents to the catalyst, and a sacrificial electron donor and proton source. Diiron complexes modeled on the active site of the [FeFe] hydrogenases[9] having the general formula $[Fe_2(\mu\text{-R})(CO)_{6-n}(L)_n]$, where commonly R = alkyl or aryl dithiolate and L = CO, CN^-, or PR_3, are a promising class of catalysts for use in photodriven H_2 production, and this has led to numerous studies of assemblies consisting of diiron complexes in combination with photosensitizers such as $Ru(bpy)_3^{2+}$ and Zn porphyrins.[2,10,11] To date, however, photoinduced electron transfer (ET) from a chromophore to a diiron hydrogenase model complex has been observed in only a handful of cases,[12−14] and the ultrafast dynamics of this process remain elusive. In many other instances, ET is inferred from the quenching of the chromophore fluorescence in the presence of the diiron complex, but this is an unreliable indicator of ET since a variety of processes can be responsible for decreases in fluorescence intensity.[15] Indeed, one of the main limitations in this field is that photoinduced ET is often thermodynamically unfavorable because of the very negative reduction potentials (≤ -1.2 V vs SCE) of most diiron complexes.

The benefits of employing a diiron complex with a mild reduction potential were highlighted in a recent report by Streich et al.,[16] in which the authors observed high catalytic turnover from solutions containing $Ru(bpy)_3^{2+}$, $[Fe_2(\mu\text{-}Cl_2bdt)(CO)_6]$ (Cl_2bdt =3,6-dichlorobenzene-1,2-dithiolate); $E_{red} = -0.80$ V[17] vs SCE), and ascorbate as a proton and electron source. Although this study clearly demonstrated the utility of diiron complexes in photodriven H_2 production, there remains a need for a greater understanding of the fundamental aspects of the ET process in diiron complex-containing systems, especially on the subnanosecond time scale. This requires covalently linked units in which the distance between the chromophore and the diiron complex as well as their relative orientation can be controlled.

Recently, naphthalene-1,8-dithiolates were shown to yield diiron proton-reduction catalysts that are both robust and redox-tunable.[18] The reduction potentials of the diiron complexes can be adjusted through chemical substitution of the naphthalene; for example, the addition of electron-withdrawing chloro substituents results in a +80 mV shift in the first reduction potential of the complex. Additionally, the authors found that the naphthalene scaffold helps to stabilize the monoanionic species relative to the analogous propane dithiolate complex $[Fe_2(\mu\text{-}S(CH_2)_3S)(CO)_6]$, as evidenced by the I_{pa}/I_{pc} ratios (~0.92 vs 0.35 for $[Fe_2(\mu\text{-}S(CH_2)_3S)(CO)_6]$) in their cyclic voltammograms.

On the basis of these findings, we reasoned that naphthalene monoimide (NMI) dithiolates would be promising ligands for diiron proton reduction catalysts in photodriven systems. The benefits of the imide functionality are twofold: First, it is a strongly electron-withdrawing substituent, which should further stabilize the monoreduced complex and result in less negative reduction potentials, making photoinduced ET from an organic chromophore (such as a Zn porphyrin) to the diiron complex thermodynamically favorable. Second, the imide serves as a convenient site for attachment of such a chromophore using well-established coupling strategies. Here we report the synthesis and spectroscopic characterization of the NMI dithiolate diiron complex NMI-$Fe_2S_2(CO)_6$ (**1**) and the Zn porphyrin−diiron complex donor−acceptor dyad ZnP−NMI-$Fe_2S_2(CO)_6$ (**2**), which was designed to undergo photoinduced intramolecular ET.

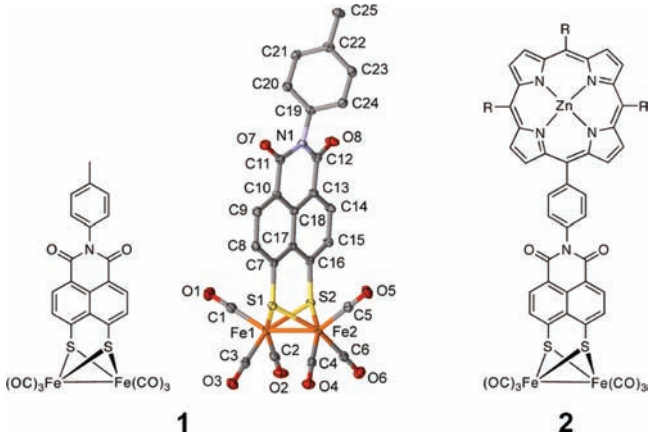

Figure 1. (left) Chemical structure of **1**. (center) X-ray structure of **1** with thermal ellipsoids set to 50% probability (see Table S1). (right) Chemical structure of **2** (R = n-C_5H_{11}).

Complex **1** was synthesized by first reacting naphthalene-1,8-dicarboxyanhydride-4,5-disulfide[19] with *p*-toluidine in refluxing pyridine in the presence of $Zn(OAc)_2$ (see the Supporting Information). The resulting NMI disulfide was reacted directly with $Fe_3(CO)_{12}$ without initial reduction to the dithiol to give the diiron complex. Complex **2** was synthesized in an analogous manner by condensation of naphthalene-1,8-dicarboxyanhydride-4,5-disulfide with 5-(*p*-aminophenyl)-10,15,20-tri-*n*-pentylporphyrin[20] and concurrent metalation of the free-base porphyrin using zinc acetate.

The X-ray structure of **1** (Figure 1) shows the characteristic Fe_2S_2 butterfly core with an Fe−Fe distance of 2.5004(3) Å. The bond lengths and angles (Table S1 in the Supporting Information) are consistent with those of naphthalene dithiolate complexes, indicating that addition of the strongly electron-withdrawing imide does not, for example, weaken the Fe−S bonds. The IR spectra of **1** and **2** are nearly identical in the carbonyl region, showing bands at 2078, 2043, and 2005 cm^{-1} (Figures S1 and S2 in the Supporting Information), which indicates that the porphyrin has no electronic interaction with the diiron core in the ground state. The carbonyl

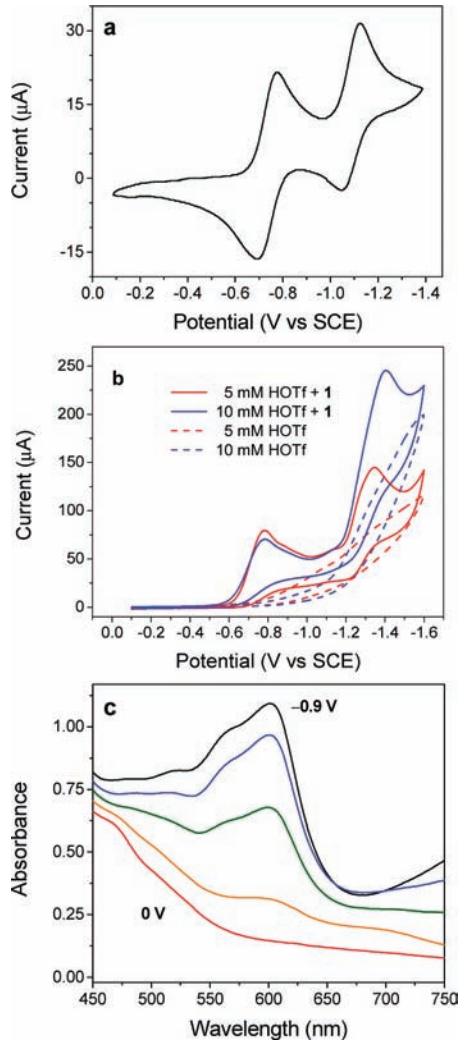

Figure 2. (a, b) Cyclic voltammograms in MeCN (0.1 M Bu_4NPF_6) at 0.1 V/s scan rate: (a) **1** (1 mM); (b) **1** (1 mM) with triflic acid (5 and 10 mM) and triflic acid alone (5 and 10 mM). (c) Absorption spectra of electrochemically generated $[NMI\text{-}Fe_2S_2(CO)_6]^{-\bullet}$ (0 to −0.9 V).

stretching frequencies of **1** and **2** are hypsochromically shifted by ∼4 cm^{-1} relative to those of the unsubstituted naphthalene dithiolate complex (here designated as complex **3**),[18] reflecting the decreased electron density at the Fe(I) centers caused by the imide.

To investigate the influence of the imide functionality on the redox properties of the diiron complex, cyclic voltammetry was performed. Complex **1** showed two quasi-reversible waves at $E_{1/2} = -0.74$ and −1.1 V (all potentials are reported vs SCE) (Figure 2a) that can be assigned to the [Fe(I)Fe(I)]/[Fe(I)Fe(0)] and [Fe(I)Fe(0)]/[Fe(0)Fe(0)] couples, respectively. First, it should be noted that, as expected, the presence of the imide resulted in reduction potentials that are significantly less negative (350−400 mV) than those of **3**. Furthermore, these values are among the most positive reported to date for a diiron hydrogenase model complex.[21] Second, the large I_{pa}/I_{pc} ratios for the first and second reductions (0.9 and 0.7, respectively) highlight the chemical stability of both the mono- and direduced species. In the presence of 5 equiv of triflic acid, the cyclic voltammogram of **1** showed an increase in current at the first reduction wave at −0.78 V and a new reduction wave at −1.4 V (Figure 2b). The first reduction wave remained irreversible in the presence of triflic acid when the scan was reversed at −0.9 V (Figure S3). When the acid concentration was increased, the current at −0.78 V remained constant while the current at −1.4 V increased, which is consistent with catalytic proton reduction.[22]

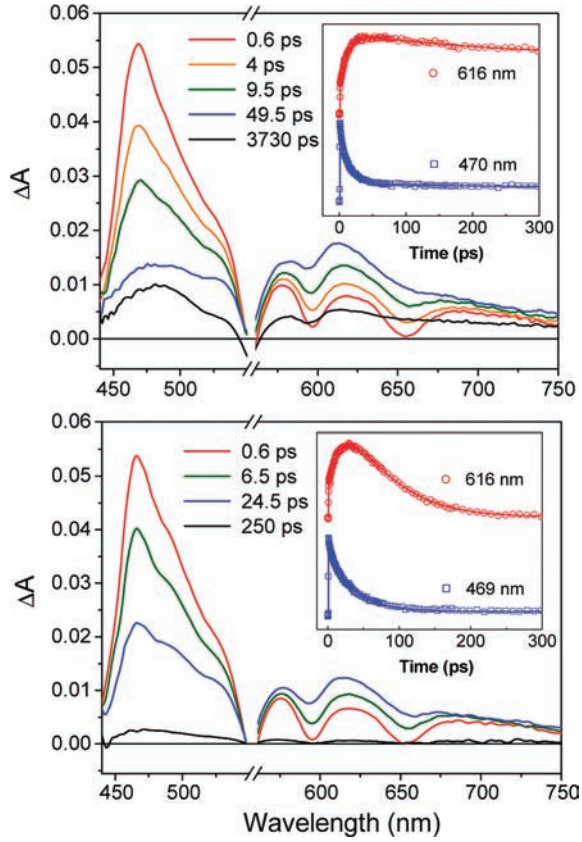

Figure 3. Transient absorption spectra of **2** in toluene (top) and CH_2Cl_2 (bottom) following excitation with 553 nm 110 fs laser pulses. The insets show the transient absorption kinetics at 616 and 470/469 nm. The spectral features monitored at these wavelengths correspond to the absorption features of $ZnP^{+\bullet}-[NMI\text{-}Fe_2S_2(CO)_6]^{-\bullet}$ and $^{1*}ZnP$, respectively. Nonlinear least-squares fits to the data are also shown.

Spectroelectrochemistry was used to obtain the UV−vis spectrum of $\mathbf{1}^{-\bullet}$ (Figure 2c), which was needed to identify the charge-separated species in the transient absorption measurements. This reduced species displays a prominent feature near 615 nm, which contrasts with the 580 and 700 nm peaks characteristic of $[Fe_2(\mu\text{-}S(CH_2)_3S)(CO)_6]^{-\bullet}$.[23] The extinction coefficient of $\mathbf{1}^{-\bullet}$ at 605 nm (ε = 13 000 M^{-1} cm^{-1}) was determined by titration of **1** with cobaltocene (Figure S4), which yielded the same spectrum as shown in Figure 2a. It should be noted that the absorption spectrum of $\mathbf{1}^{-\bullet}$ is also significantly different from that of $NMI^{-\bullet}$,[24] indicating that the electron density is localized at the $Fe_2S_2(CO)_6$ core of **1** and not on the NMI moiety. This is consistent with the observation that **1** is reduced at −0.74 V versus SCE while NMI itself is reduced at −1.37 V versus SCE[24] as well as with the results of semiempirical unrestricted PM3 calculations on $\mathbf{1}^{-\bullet}$ (Figure S5).

The free energy for photoinduced charge separation (CS) in the Zn porphyrin−diiron complex dyad **2** was estimated to be ΔG_{CS} = −0.13 eV in toluene and −0.63 eV in CH_2Cl_2 (see the Supporting Information). These estimates were based on the first reduction potential of **1**, the reversible oxidation potential ($E_{1/2}$ = 0.62 V), and the excited-state energy (S_1 = 2.06 eV) of Zn 5,10,15-tri-*n*-pentyl-20-phenylporphyrin (ZnP), with corrections for the ion-pair solvation and Coulombic energies. ZnP within **2** was selectively photoexcited at its 553 nm Q band (Figure S6) with 110 fs laser pulses, as **1** has negligible absorbance at that wavelength (Figure S7). Figure 3 shows the transient absorption spectra of **2** in toluene

and CH_2Cl_2 at various time delays, and the corresponding transient absorption kinetics are shown in the insets. At times <1 ps after photoexcitation, the transient spectra are characteristic of ^{1*}ZnP, with a strong absorption at 470 nm and broad features from 550−800 nm superimposed on the bleach of the ground-state absorption along with a stimulated emission feature at 655 nm. The spectra evolve in time to develop a distinct peak at 616 nm, which is assigned to $[NMI\text{-}Fe_2S_2(CO)_6]^{-\bullet}$ on the basis of the data shown in Figure 2c and Figure S4. The broad features due to $ZnP^{+\bullet}$ are characteristically indistinct,[25] so the 616 nm peak was used to monitor the CS and charge recombination (CR) dynamics of **2**, which yielded $\tau_{CS} = 12 \pm 1$ ps and $\tau_{CR} = 3.0 \pm 0.2$ ns in toluene and $\tau_{CS} = 24 \pm 1$ ps and $\tau_{CR} = 57 \pm 1$ ps in CH_2Cl_2. These time constants are consistent with the expectations of Marcus ET theory, and similar solvent dependencies have been observed for other donor−acceptor systems.[20] Photoexcitation of the disulfide precursor to **2** (ZnP-$NMIS_2$; see the Supporting Information for the chemical structure) in both toluene and CH_2Cl_2 produced only ^{1*}ZnP and ^{3*}ZnP (Figures S8 and S9), showing that ET is favorable only when the diiron complex is present. Photoinduced ET in our dyad system was therefore unequivocally identified by the observation of $ZnP^{+\bullet}$−$[NMI\text{-}Fe_2S_2(CO)_6]^{-\bullet}$ after the initial formation of ^{1*}ZnP. The observed ΔA values and kinetics showed that the quantum yield for the formation of $ZnP^{+\bullet}$−$[NMI\text{-}Fe_2S_2(CO)_6]^{-\bullet}$ is approximately unity in both toluene and CH_2Cl_2 (see the Supporting Information).

At long delay times, the transient spectra of **2** in toluene show that CR produced ^{3*}ZnP, as evidenced by the shift of the transient feature at 470 nm to 480 nm and the persistence of the transient absorption changes at times >6 ns (Figure 3 and Figure S10). In contrast, ^{3*}ZnP did not form upon CR in CH_2Cl_2. Ultrafast formation of $ZnP^{+\bullet}$−$[NMI\text{-}Fe_2S_2(CO)_6]^{-\bullet}$ precluded significant yields of ^{3*}ZnP resulting from spin−orbit-induced intersystem crossing, which is much slower (2.3 ns).[20] However, the initial formation of $ZnP^{+\bullet}$−$[NMI\text{-}Fe_2S_2(CO)_6]^{-\bullet}$ was most likely followed by radical-pair intersystem crossing (RP-ISC) driven by rapid spin relaxation at the reduced paramagnetic diiron complex. If the energy of the resulting triplet radical ion pair is above that of ^{3*}ZnP ($E_T = 1.58$ eV),[26] charge recombination should produce significant yields of the porphyrin triplet. The energies of $ZnP^{+\bullet}$−$[NMI\text{-}Fe_2S_2(CO)_6]^{-\bullet}$ in toluene and CH_2Cl_2 are 1.93 and 1.43 eV, respectively (see the Supporting Information), so CR to form ^{3*}ZnP is thermodynamically accessible only in toluene.

Photochemical hydrogen evolution experiments were performed by irradiating **2** (2 μmol) in the presence of trifluoroacetic acid (TFA) (2 mmol) in toluene with 500−800 nm light (see the Supporting Information). Hydrogen gas (0.9 μmol) was generated and quantified relative to a gas calibration standard by GC. In the absence of either TFA or light, no H_2 was detected. However, photochemical H_2 generation from TFA using **2** was not catalytic (turnover number of ~0.5). Addition of a *p*-anisidine sacrificial donor (2 mmol) significantly decreased the H_2 formation (0.02 μmol), which can be attributed to *p*-anisidine protonation, greatly diminishing both its electron donor ability and the TFA concentration.

In conclusion, the NMI dithiolate scaffold is a potentially important building block in the development of covalent arrays for the study of photodriven ET in diiron complex-containing systems. We are currently investigating ways to improve the photocatalytic performance by, for example, incorporating sacrificial donors that are able to reduce relatively stable cation radicals in acidic media and extending the lifetime of the charge-separated state.

Acknowledgment. We thank M. T. Vagnini for nanosecond spectroscopic measurements and Profs. T. Rauchfuss (U. of Illinois Urbana−Champaign) and R. Eisenberg (U. of Rochester) for helpful discussions. This work was supported as part of the ANSER Center, an Energy Frontier Research Center funded by the U.S. Department of Energy, Office of Science, Office of Basic Energy Sciences, under Award DE-SC0001059.

Supporting Information Available: Experimental details, including the synthesis and characterization of **1** and **2**; transient absorption spectra; structural data; H_2 formation; and a CIF for **1**. This material is available free of charge via the Internet at http://pubs.acs.org.

References

(1) Gloaguen, F.; Rauchfuss, T. B. *Chem. Soc. Rev.* **2009**, *38*, 100.
(2) Wang, M.; Na, Y.; Gorlov, M.; Sun, L. *Dalton Trans.* **2009**, 6458.
(3) Lazarides, T.; McCormick, T.; Du, P.; Luo, G.; Lindley, B.; Eisenberg, R. *J. Am. Chem. Soc.* **2009**, *131*, 9192.
(4) Reisner, E.; Powell, D. J.; Cavazza, C.; Fontecilla-Camps, J. C.; Armstrong, F. A. *J. Am. Chem. Soc.* **2009**, *131*, 18457.
(5) Gärtner, F.; Sundararaju, B.; Surkus, A.-E.; Boddien, A.; Loges, B.; Junge, H.; Dixneuf, P. H.; Beller, M. *Angew. Chem., Int. Ed.* **2009**, *48*, 9962.
(6) Jacobsen, G. M.; Yang, J. Y.; Twamley, B.; Wilson, A. D.; Bullock, R. M.; DuBois, M. R.; DuBois, D. L. *Energy Environ. Sci.* **2008**, *1*, 167.
(7) Wilson, A. D.; Shoemaker, R. K.; Miedaner, A.; Muckerman, J. T.; DuBois, D. L.; DuBois, M. R. *Proc. Natl. Acad. Sci. U.S.A.* **2007**, *104*, 6951.
(8) Hu, X.; Brunschwig, B. S.; Peters, J. C. *J. Am. Chem. Soc.* **2007**, *129*, 8988.
(9) Peters, J. W.; Lanzilotta, W. N.; Lemon, B. J.; Seefeldt, L. C. *Science* **1998**, *282*, 1853.
(10) Tard, C.; Pickett, C. J. *Chem. Rev.* **2009**, *109*, 2245.
(11) Sun, L.; Åkermark, B.; Ott, S. *Coord. Chem. Rev.* **2005**, *249*, 1653.
(12) Na, Y.; Pan, J.; Wang, M.; Sun, L. *Inorg. Chem.* **2007**, *46*, 3813.
(13) Na, Y.; Wang, M.; Pan, J.; Zhang, P.; Åkermark, B.; Sun, L. *Inorg. Chem.* **2008**, *47*, 2805.
(14) Li, X.; Wang, M.; Zhang, S.; Pan, J.; Na, Y.; Liu, J.; Åkermark, B.; Sun, L. *J. Phys. Chem. B* **2008**, *112*, 8198.
(15) Lakowicz, J. R. *Principles of Fluorescence Spectroscopy*; Kluwer: Dordrecht, The Netherlands, 1999.
(16) Streich, D.; Astuti, Y.; Orlandi, M.; Schwartz, L.; Lomoth, R.; Hammarström, L.; Ott, S. *Chem.—Eur. J.* **2010**, *16*, 60.
(17) Schwartz, L.; Singh, P. S.; Eriksson, L.; Lomoth, R.; Ott, S. *C. R. Chim.* **2008**, *11*, 875.
(18) Wright, R. J.; Lim, C.; Tilley, T. D. *Chem.—Eur. J.* **2009**, *15*, 8518.
(19) Tesmer, M.; Vahrenkamp, H. *Eur. J. Inorg. Chem.* **2001**, 1183.
(20) Kelley, R. F.; Tauber, M. J.; Wasielewski, M. R. *J. Am. Chem. Soc.* **2006**, *128*, 4779.
(21) Felton, G. A. N.; Mebi, C. A.; Petro, B. J.; Vannucci, A. K.; Evans, D. H.; Glass, R. S.; Lichtenberger, D. L. *J. Organomet. Chem.* **2009**, *694*, 2681.
(22) Gloaguen, F.; Lawrence, J. D.; Rauchfuss, T. B. *J. Am. Chem. Soc.* **2001**, *123*, 9476.
(23) Borg, S. J.; Behrsing, T.; Best, S. P.; Razavet, M.; Liu, X.; Pickett, C. J. *J. Am. Chem. Soc.* **2004**, *126*, 16988.
(24) Gosztola, D.; Niemczyk, M. P.; Svec, W.; Lukas, A. S.; Wasielewski, M. R. *J. Phys. Chem. A* **2000**, *104*, 6545.
(25) Hayes, R. T.; Wasielewski, M. R.; Gosztola, D. *J. Am. Chem. Soc.* **2000**, *122*, 5563.
(26) Wasielewski, M. R.; Johnson, D. G.; Svec, W. A.; Kersey, K. M.; Minsek, D. W. *J. Am. Chem. Soc.* **1988**, *110*, 7219.

JA100016V